Science Advances
AAAS

Supplementary Materials for

Cryo-EM structure and regulation of human NAD kinase

Prakash P. Praharaj *et al.*

Corresponding author: Gilles Labesse, labesse@cbs.cnrs.fr; Gerta Hoxhaj, gerta.hoxhaj@utsouthwestern.edu

Sci. Adv. **11**, eads2664 (2025)
DOI: 10.1126/sciadv.ads2664

This PDF file includes:

Table S1. Post-translational modifications of NADK expressed in HEK-293 cells.

Site	Peptide Sequence	PhosphoPeptide modifications	Abundance of modification (10^6)	Total peptide abundance (10^6)	% modified peptide	Phosphosite®
S15	MTMNKESPDAAAYCCSACHGDETWSYNHPIR	1xPhospho [S8]	23.431	181.948	12.88	3HTP
S15	ELSPDAAAYCCSACHGDETWSYNHPIR	1xPhospho [S3]	350.63	6896.52	5.08	3HTP
S15	ELSPDAAAYCCSACHGDETWSYNHPIRGR	1xPhospho [S3]	37.426	1849.1	2.02	3HTP
S15, S24	ELSPDAAAYCCSACHGDETWSYNHPIR	2xPhospho [S3; S12]	0.184	6896.52	0.0027	
S44	AKSRSLSASPALGSTK	1xPhospho [S3]	ND	2.097		10HTP
S46	SRSLSASPALGSTKEFR	1xPhospho [S3]	0.537	0.537	100	30HTP
S46	SRSLSASPALGSTK	1xPhospho [S3]	80.528	429.29	18.76	30HTP
S44, S46	AKSRSLSASPALGSTK	2xPhospho [S3; S5]	2.097	2.097	100	
S48	SLSASPALGSTKEFRR	1xPhospho [S3]	3.161	93.74	3.37	37HTP
S46; S48	SRSLSASPALGSTK	2xPhospho [S3; S5]	103.22	429.29	24.04	
S48; S50	SLSASPALGSTK	2xPhospho [S3; S5]	64.916	12857.7	0.5	
S46; S48; S50	SRSLSASPALGSTK	3xPhospho [S3; S5; S7]	ND	429.29		
S64	TRSLHGPCPVTTFGPKACVLQNPQTIMHIQDPASQR	1xPhospho [S3]	0.94	5.224	17.99	44HTP
S64	TRSLHGPCPVTTFGPK	1xPhospho [S3]	550.51	554.56	99.27	44HTP
S64	SLHGPCPVTTFGPK	1xPhospho [S1]	145.59	20746	0.702	44HTP
T62; S64; T/S	TRSLHGPCPVTTFGPKACVLQNPQTIMHIQDPASQR	3xPhospho [T1; S3; T/S]	0.96	5.224	18.378	
S117	MRDASLLQPFK	1xPhospho [S5]	29.61	2227.72	1.33	
S117	DASLLQPFK	1xPhospho [S3]	49.97	18432.1	0.27	
S117	DASLLQPFKELCTHLMEENMIVYVEK	1xPhospho [S3]	2.64	869.8	0.3	
S153	KVLEDPAIASDESFGAVK	1xPhospho [S13]	ND	5316.8		
S153	VLEDPAIASDESFGAVK	1xPhospho [S12]	ND	23471.5		
S371	IMLSPEAR	1xPhospho [S4]	10.15	21843.4	0.05	
S395	HGDSISITTSCYPLPSICVR	1xPhospho [S4]	2.0	5930.09	0.03	

Site	Peptide Sequence	Methylation events	Abundance of modification (10^6)	Total peptide abundance (10^6)	% modified peptide	Phosphosite®
K12	MTMNKELSPDAAAYCCSACHGDETWSYNHPIR	1xTrimethyl [K5]	77.5	181.948	42.59	
K12	MTMNKELSPDAAAYCCSACHGDETWSYNHPIR	1xDimethyl [K5]	ND	181.948		
K12, T9	MTMNKELSPDAAAYCCSACHGDETWSYNHPIR	1xDimethyl [K5]; 1xPhospho [T2]	ND	181.948		
R39	ELSPDAAAYCCSACHGDETWSYNHPIRGRAK	1xDimethyl [R27]	4.52	4.52	100	3HTP
R41	ELSPDAAAYCCSACHGDETWSYNHPIRGRAK	1xTrimethyl [R29]	1.74	1.74	100	5HTP
K43	AKSRSLSASPALGSTK	1xTrimethyl [K2]	ND	2.097		
R45	AKSRSLSASPALGSTK	1xDimethyl [R4]	ND	2.097		
R45	SRSLSASPALGSTK	1xMethyl [R2]	182.34	429.29	42.48	1HTP
R45	SRSLSASPALGSTK	1xDimethyl [R2]	44.709	429.29	10.41	1HTP
K57	SLSASPALGSTKEFR	1xMethyl [K12]	1.176	12857.7	0.01	
K77	TRSLHGPCPVTTFGPKACVLQNPQTIMHIQDPASQR	1xTrimethyl [K16]; 1xPhospho [T/S]	ND	5.224		
K77	SLHGPCPVTTFGPKACVLQNPQTIMHIQDPASQR	1xDimethyl [K14]	17.75	408.04	4.35	
K77	SLHGPCPVTTFGPKACVLQNPQTIMHIQDPASQR	1xTrimethyl [K14]	93.71	408.04	22.97	
R97	ACVLQNPQTIMHIQDPASQR	1xDimethyl [R20]	ND	26137.2		
K123	DASLLQPFKELCTHLMEENMIVYVEK	1xTrimethyl [K9]	ND	869.8		
K140	ELCTHLMEENMIVYVEK	1xDimethyl [K17]	ND	15711.6		
K141	KVLEDPAIASDESFGAVK	1xMethyl [K1]	116.68	5316.8	2.19	
K141	KVLEDPAIASDESFGAVK	1xTrimethyl [K1]	2.245	5316.8	0.04	
K141	KVLEDPAIASDESFGAVKK	1xMethyl [K1]	4.53	743.82	0.61	
K141	KVLEDPAIASDESFGAVKK	1xDimethyl [K1]	ND	743.82		
K158	VLEDPAIASDESFGAVK	1xMethyl [K17]	121.53	23471.5	0.52	
K158	VLEDPAIASDESFGAVKK	1xTrimethyl [K17]	5.74	3100.82	0.19	
K158	VLEDPAIASDESFGAVKK	1xMethyl [K17]	6.39	3100.82	0.21	
K158; K159; K160	KVLEDPAIASDESFGAVKKK	3xMethyl [K18; K19; K20]	ND	6.16		

R290	QAMQYQVLNEVVIDR	1xMethyl [R15]	4.69	8198.9	0.06	
Site	**Peptide Sequence**	**Acetylation events**	**Abundance of modification (10^6)**	**Total peptide abundance (10^6)**	**% modified peptide**	**Phosphosite®**
K12	MTMNKESPDAAAYCCSACHGDETWSYNHPIR	1xAcetyl [K5]	79.445	181.948	43.66	
K43	AKSRSLSASPALGSTK	1xAcetyl [K2]	ND	2.097		
K57	SLSASPALGSTK	1xAcetyl [K12]	9.69	12857.7	0.08	2HTP
K77	SLHGPCPVTTFGPKACVLQNPQTIMHIQDPASQR	1xAcetyl [K14]	61.67	408.04	15.11	
T62; K77	TRSLHGPCPVTTFGPKACVLQNPQTIMHIQDPASQR	1xPhospho [T1]; 1xAcetyl [K16]	3.324	5.224	63.623	
S64; K77	TRSLHGPCPVTTFGPKACVLQNPQTIMHIQDPASQR	1xPhospho [S3]; 1xAcetyl [K16]	ND	5.224		
K102	LTWNKSPK	1xAcetyl [K5]	42.51	154.7	27.48	
K105	SPKSVLVIK	1xAcetyl [K3]	71.54	191.56	37.35	
K111	SVLVIKK	1xAcetyl [K6]	64.42	64.42	100	
K140	ELCTHLMEENMIVYVEKK	1xAcetyl [K17]	6.64	259.07	2.56	
K141	KVLEDPAIASDESFGAVK	1xAcetyl [K1]	20.94	5316.8	0.39	
K158	KVLEDPAIASDESFGAVKK	1xAcetyl [K18]	14.35	743.82	1.93	1HTP
K158	VLEDPAIASDESFGAVK	1xAcetyl [K17]	3.79	23471.5	0.02	1HTP
K158	VLEDPAIASDESFGAVKK	1xAcetyl [K17]	27.38	3100.82	0.88	1HTP
K158	VLEDPAIASDESFGAVKK	1xMethyl [K17]	6.39	3100.82	0.21	1HTP

A

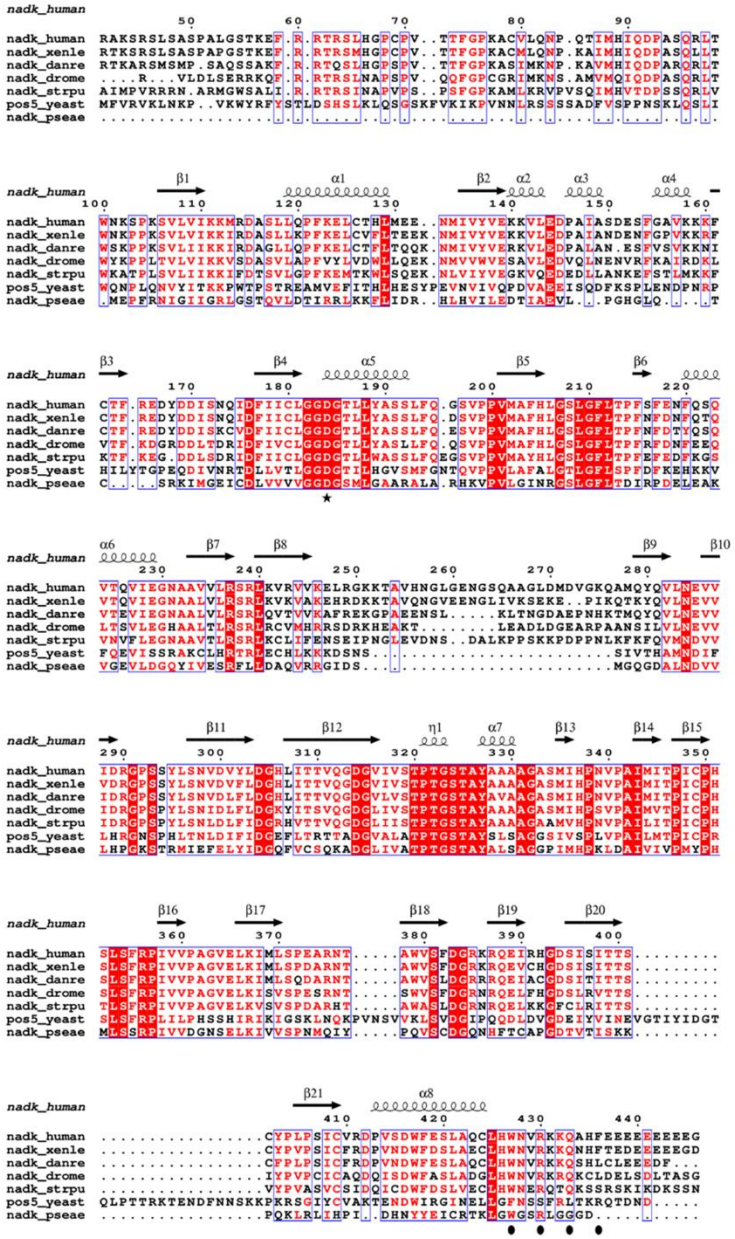
nadk_human
nadk_xenle
nadk_danre
nadk_drome
nadk_strpu
pos5_yeast
nadk_pseae

B

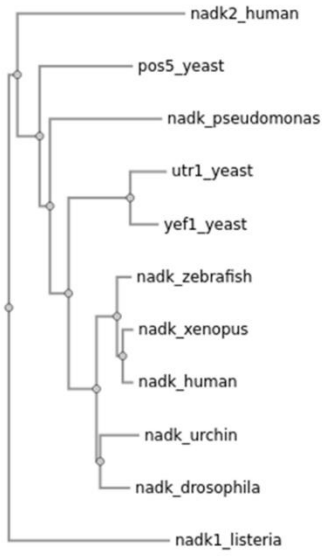
nadk2_human
pos5_yeast
nadk_pseudomonas
utr1_yeast
yef1_yeast
nadk_zebrafish
nadk_xenopus
nadk_human
nadk_urchin
nadk_drosophila
nadk1_listeria

Fig. S1. Comparative sequence alignment and phylogenetic analysis of NADKs.

(**A**) Sequence alignment of NADKs. A multiple sequence alignment shown of cytosolic NADKs from representative animals (human: nadk_human, Xenopus: nadk_xenle, zebrafish: nadk_danre, drosophila: nadk_drome and see urchin: nadk_strpu), alongside the mitochondrial NADK from yeast (pos5_yeast) and from a bacterial pathogen, *Pseudomonas aeruginosa* (nadk_pseae). The catalytic aspartate is highlighted with a black star, and the functionally important residues from the C-tail (this study) are shown in black circle. The figure was generated using Espript (https://espript.ibcp.fr/ESPript/ESPript/).

(**B**) Evolution of NADKs. A phylogenic tree of various NADKs was built using the software Ibis2Analyzer (http://ibis2analyzer.lcqb.upmc.fr/). Cytosolic NADKs from animals appear more closely related to those NADKs from gram (-) bacteria, than the human mitochondrial NADK2 (nadk2_human).

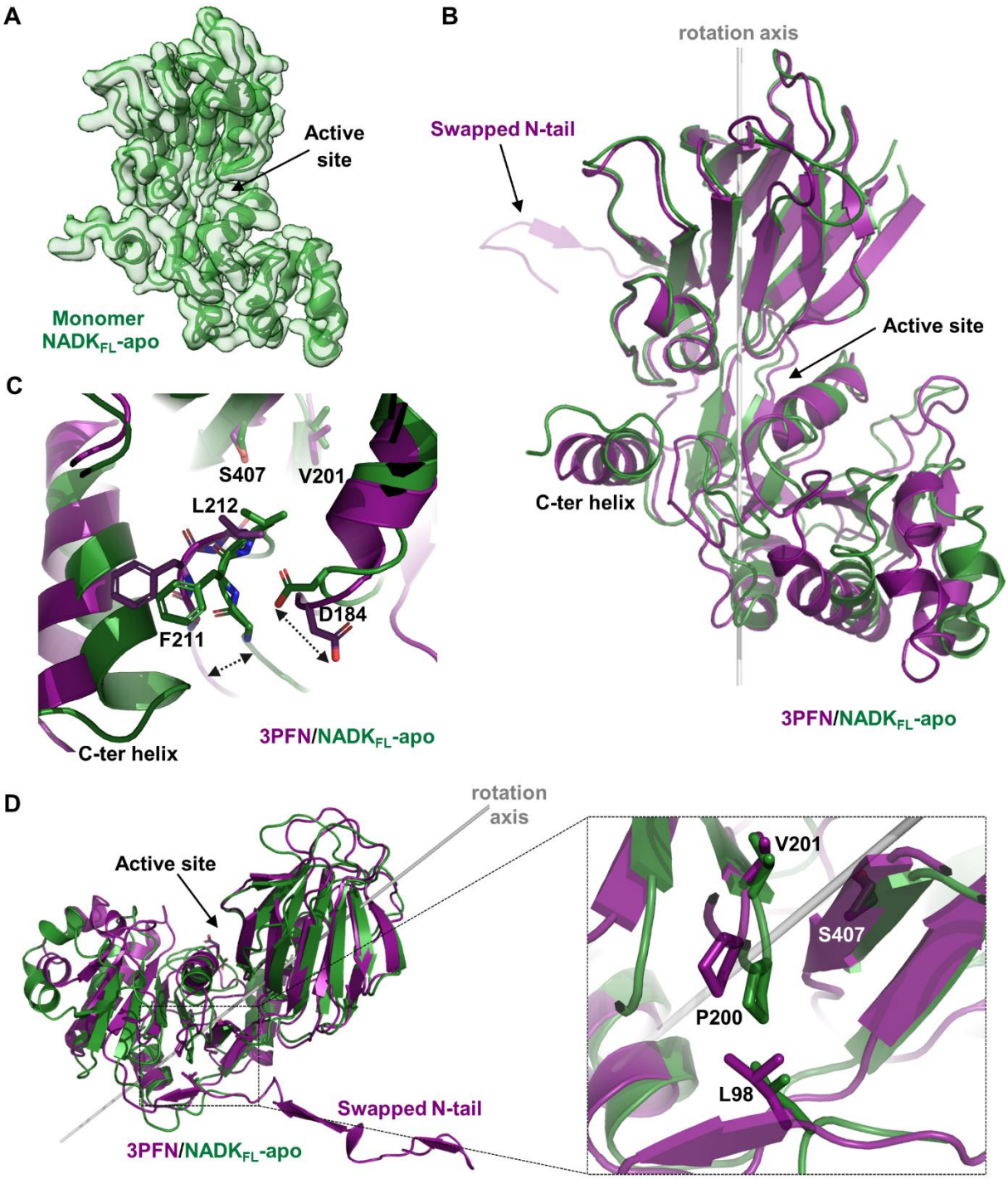
A
Active site
Monomer
NADK$_{FL}$-apo
B
rotation axis
Swapped N-tail
Active site
C-ter helix
3PFN/NADK$_{FL}$-apo
C
S407
V201
L212
D184
F211
C-ter helix
3PFN/NADK$_{FL}$-apo
D
rotation axis
Active site
Swapped N-tail
3PFN/NADK$_{FL}$-apo
V201
S407
P200
L98

Figure S2: Comparative analysis of the cryo-EM full-length $NADK_{FL}$ and crystal structure of a truncated hsNADK

(**A**) Electron density and molecular model of a monomer of apo $NADK_{FL}$.

(**B**) Comparison of apo $NADK_{FL}$ cryo-EM monomer in green and that of the crystal structure of a truncated construct of hsNADK (PDB3PFN) in violet. The main rotation axis is shown in light grey.

(**C**) Comparison of the active sites of apo $NADK_{FL}$ and the crystal structure 3PFN. Zoom of the core of the catalytic domains showing the positions of the two pivots, namely V201 and S407, and two highly conserved residues, F211 and L212. The re-orientation of the catalytic aspartate D184 and its interactions with the backbone nitrogens of F211 and L212 are shown. Same color code as in (B).

(**D**) Interaction network connecting the N-tail (especially L98) and the hinge pivots (V201 and S407) through proline P200 in hsNADK (3PFN) and $NADK_{FL}$ cryo-EM structure (color coded as in B). Panels B-D were drawn using PyMOL.

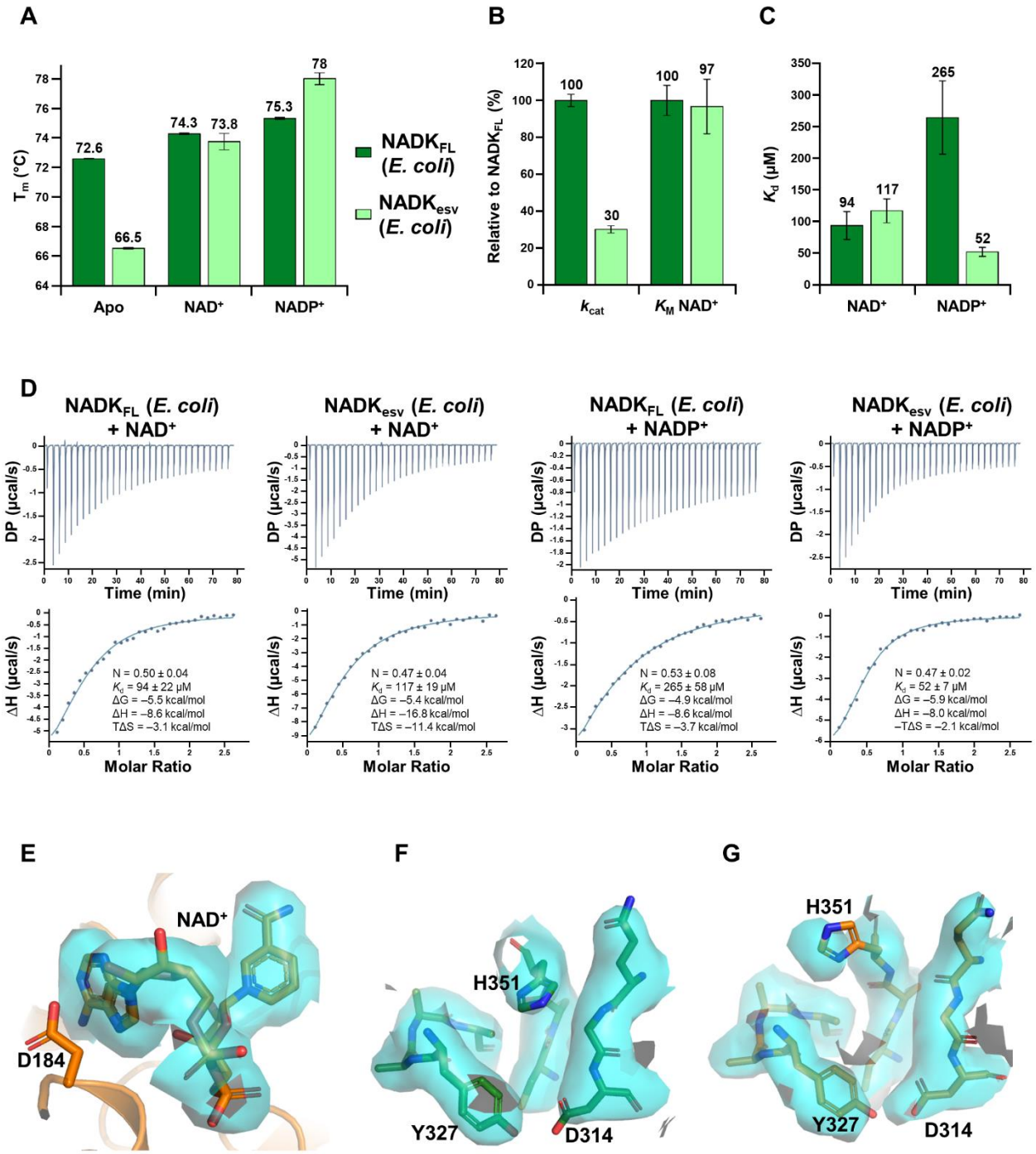
A
B
C
D
E
F
G
T_m (°C)
72.6
66.5
74.3
73.8
75.3
78
Apo
NAD+
NADP+
NADK$_{FL}$ (*E. coli*)
NADK$_{esv}$ (*E. coli*)
Relative to NADK$_{FL}$ (%)
100
30
100
97
k_{cat}
K_M NAD+
K_d (μM)
94
117
265
52
NADK$_{FL}$ (*E. coli*) + NAD+
NADK$_{esv}$ (*E. coli*) + NAD+
NADK$_{FL}$ (*E. coli*) + NADP+
NADK$_{esv}$ (*E. coli*) + NADP+
DP (μcal/s)
Time (min)
ΔH (μcal/s)
Molar Ratio
N = 0.50 ± 0.04
K_d = 94 ± 22 μM
ΔG = –5.5 kcal/mol
ΔH = –8.6 kcal/mol
TΔS = –3.1 kcal/mol
N = 0.47 ± 0.04
K_d = 117 ± 19 μM
ΔG = –5.4 kcal/mol
ΔH = –16.8 kcal/mol
TΔS = –11.4 kcal/mol
N = 0.53 ± 0.08
K_d = 265 ± 58 μM
ΔG = –4.9 kcal/mol
ΔH = –8.6 kcal/mol
TΔS = –3.7 kcal/mol
N = 0.47 ± 0.02
K_d = 52 ± 7 μM
ΔG = –5.9 kcal/mol
ΔH = –8.0 kcal/mol
–TΔS = –2.1 kcal/mol
NAD+
D184
H351
Y327
D314
H351
Y327
D314

Figure S3: Biochemical characterization of hsNADK

(**A**) Thermal stability of $NADK_{FL}$ (dark green) and $NADK_{esv}$ (light green) in its apo form and in complex with NAD^+ or $NADP^+$.

(**B**) Relative kinetic parameters, steady state rate constant and Michaelis constant of $NADK_{esv}$ compared to $NADK_{FL}$ for NAD^+ (color code as in A).

(**C**) Dissociation constants of NAD^+ or $NADP^+$ from $NADK_{FL}$ and $NADK_{esv}$ (color code as in A).

(**D**) ITC isotherms for the binding of NAD^+ and $NADP^+$ to $NADK_{FL}$ or $NADK_{esv}$ are shown. Values deduced from the isotherms are displayed under each curve.

(E) The electron density for the NAD^+ molecule bound to $NADK_{esv}$ is shown in cyan surface. The ligand and the side chain of D184 are shown in sticks.

(**F**) Electron density and model of the active site around histidine H351 in the apo-form of $NADK_{FL}$. The electron density is shown in cyan surface, and protein residues are shown in dark green sticks.

(G) Electron density and model of the active site around histidine H351 in the NAD^+-bound form of $NADK_{esv}$. The electron density is shown in cyan surface, and protein residues are shown in orange sticks.

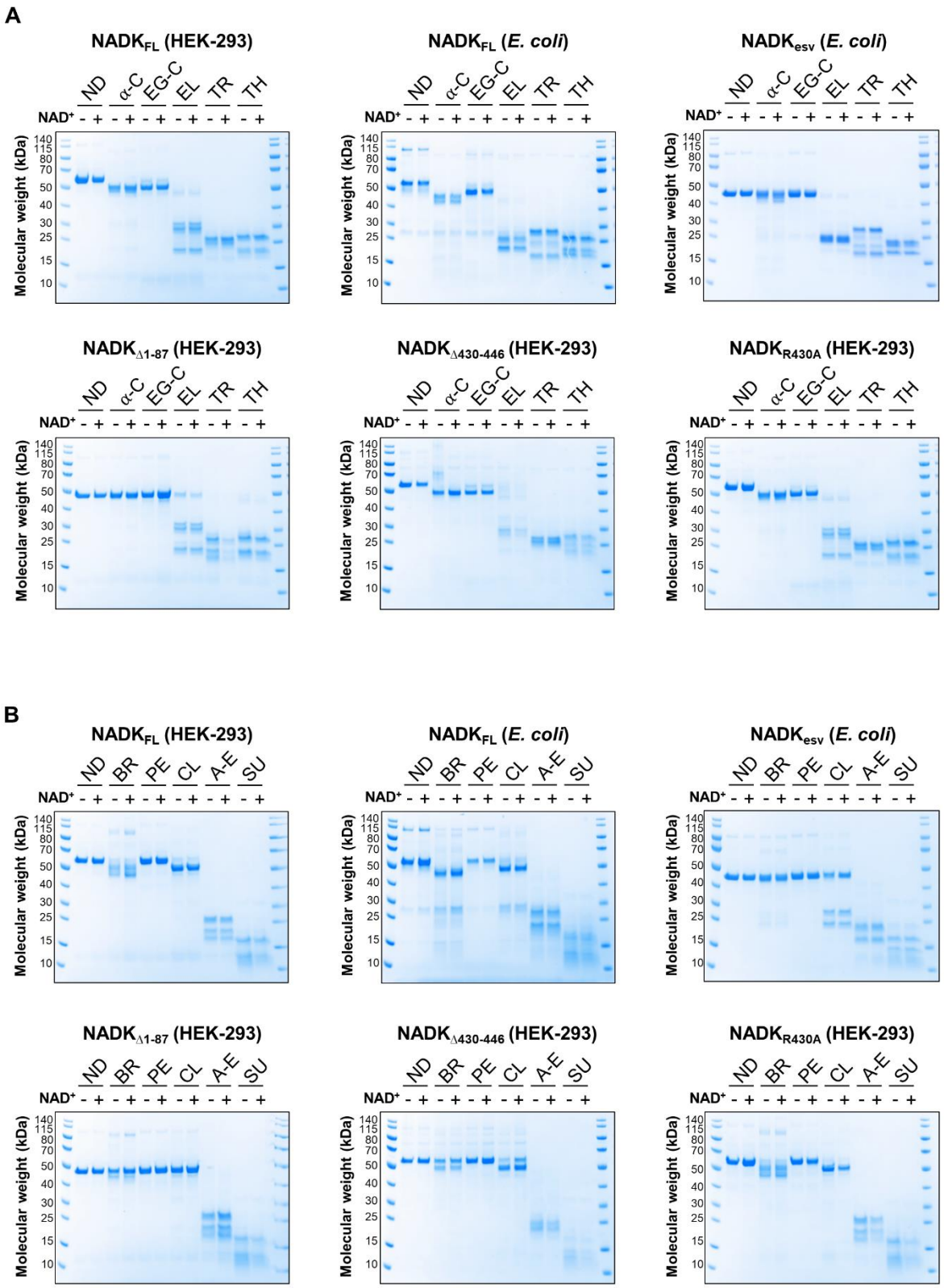
A
NADK$_{FL}$ (HEK-293)
NADK$_{FL}$ (*E. coli*)
NADK$_{esv}$ (*E. coli*)
NADK$_{\Delta 1\text{-}87}$ (HEK-293)
NADK$_{\Delta 430\text{-}446}$ (HEK-293)
NADK$_{R430A}$ (HEK-293)
ND
α-C
EG-C
EL
TR
TH
NAD+
Molecular weight (kDa)
140
115
80
70
50
40
30
25
15
10
B
NADK$_{FL}$ (HEK-293)
NADK$_{FL}$ (*E. coli*)
NADK$_{esv}$ (*E. coli*)
NADK$_{\Delta 1\text{-}87}$ (HEK-293)
NADK$_{\Delta 430\text{-}446}$ (HEK-293)
NADK$_{R430A}$ (HEK-293)
ND
BR
PE
CL
A-E
SU
NAD+
Molecular weight (kDa)

Figure S4: Proteolysis profiles of various hsNADK constructs.

(**A, B**) A panel of diluted proteases was used to partially digest (1 hour) different hsNADK constructs (purified from mammalian cells or bacteria), followed by analysis with SDS-PAGE gels. Constructs labeled as described in the text: $NADK_{FL}$ (HEK-293), $NADK_{FL}$ (*E. coli*), $NADK_{esv}$ (*E. coli*), NADK $_{\Delta 1\text{-}87}$ (HEK-293), $NADK_{\Delta 430\text{-}446}$ (HEK-293), and $NADK_{R430A}$ (HEK-293) were treated with the indicated proteases. Proteases used include ND = Not Digested, α-C = α-Chymotrypsin, EG-C = Endoproteinase Glu-C, EL = Elastase, TR = Trypsin, TH = Thermolysin Br = Bromelain, PE = Pepsin, CL = Clostripain, A-E = Actinase-E, SU = Subtilisin.

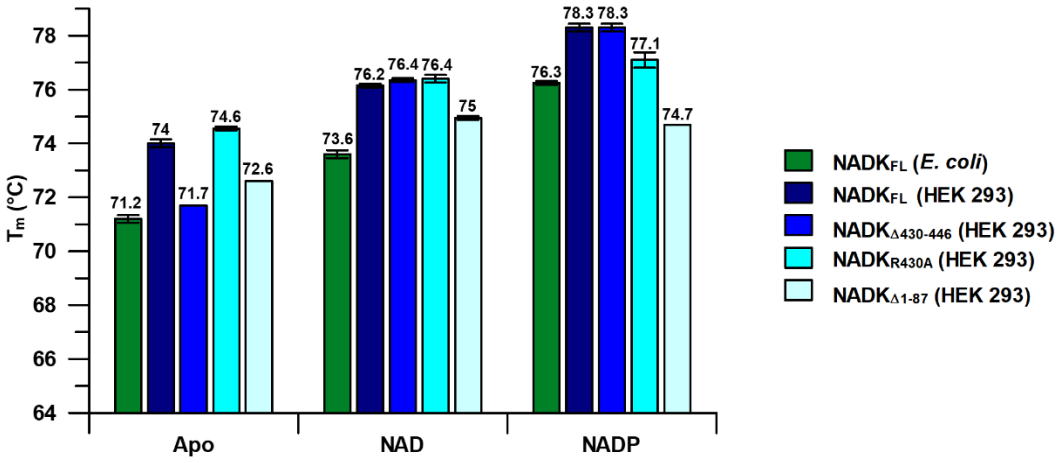

Figure S5: Thermal stability of various hsNADK constructs.

The thermostability of $NADK_{FL}$ purified from bacteria (dark green) and HEK-293 cells (dark blue) is compared with that of several hs$NADK_{FL}$ mutants purified from HEK-293 cells, both in the absence and presence of ligands (NAD^+ or $NADP^+$).

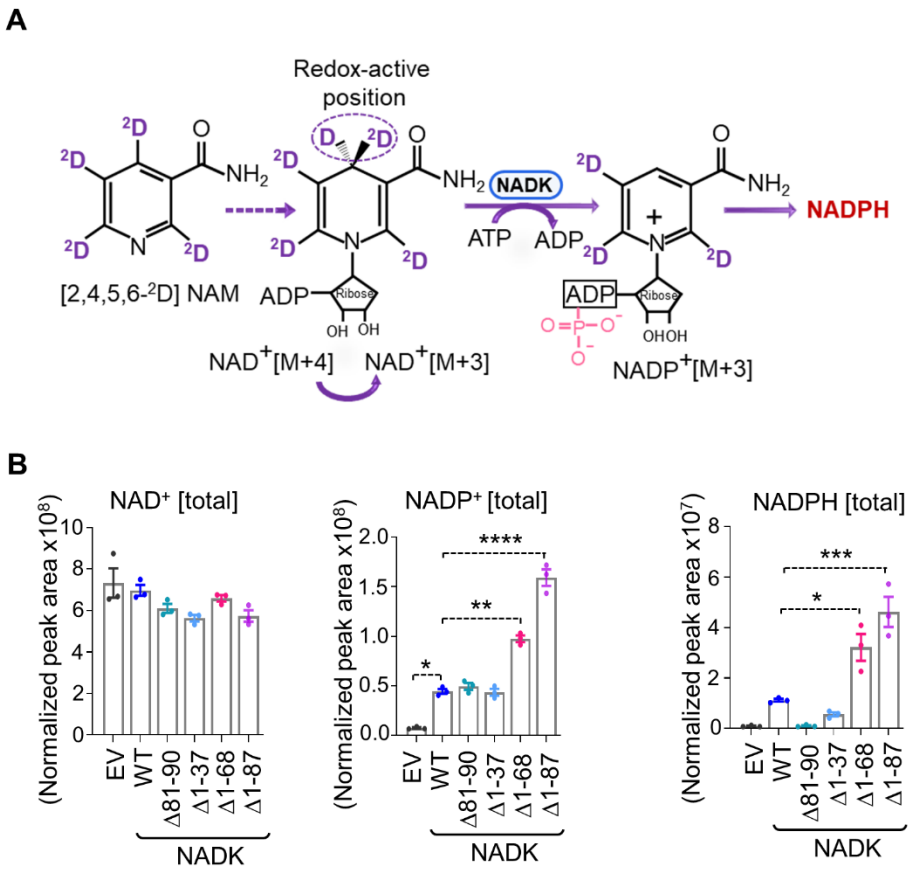

Fig. S6. Impact of the N-terminal deletions on cellular NAD(P)(H) pools.

(**A**) Schematics of labeling of NAD^+ and $NADP^+$ from $^2D_4$-nicotinamide. Redox-active positions are indicated.

(**B**) Normalized peak areas showing total NAD^+, $NADP^+$, and NADPH pools from NADK-deficient HEK-293 cells expressing either empty vector (EV) or the indicated NADK variants (WT, Δ1-37, Δ1-68, Δ1-87, Δ81-90, and ISO3). All the data are shown as the mean ± S.E.M. of biological triplicates from at least two independent experiments. $*p < 0.05$, $**p < 0.01$, $***p < 0.001$, $****p < 0.0001$ were calculated with one-way ANOVA and Sidak Post-hoc test.

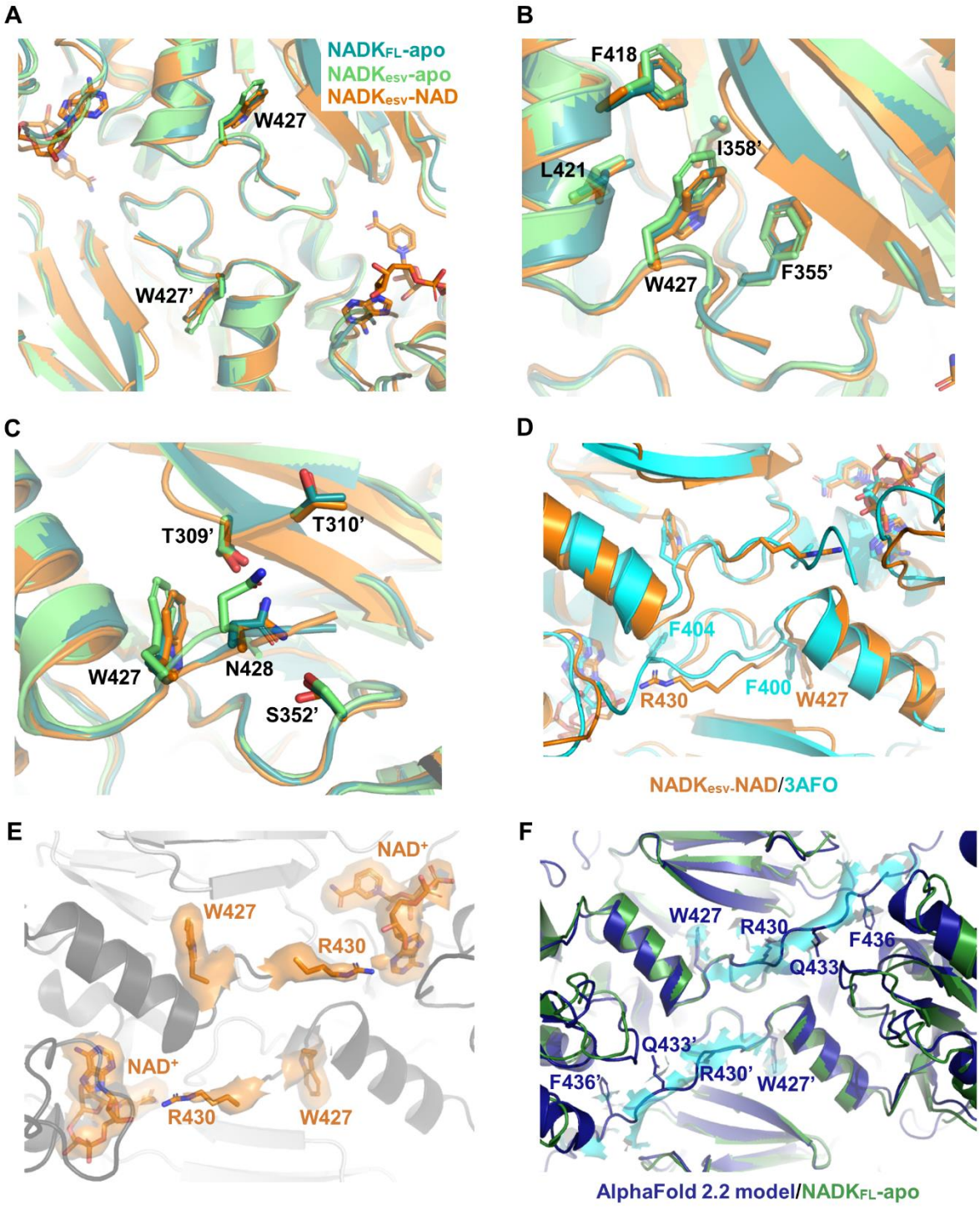
A
NADKFL-apo
NADKesv-apo
NADKesv-NAD
W427
W427'
B
F418
I358'
L421
W427
F355'
C
T309'
T310'
W427
N428
S352'
D
F404
R430
F400
W427
NADKesv-NAD/3AFO
E
NAD+
W427
R430
NAD+
R430
W427
F
W427
R430
F436
Q433
Q433'
F436'
R430'
W427'
AlphaFold 2.2 model/NADKFL-apo

Figure S7. Structural analysis of the C-terminal tail of NADK

(**A**) Zoom in the C-terminal region of the hsNADK. Comparison of the three cryo-EM structure hsNADK$_{FL}$-apo (teal), hsNADK$_{esv}$-apo (green), and hsNADK$_{esv}$-NAD$^+$ (orange). These structures highlight the positioning of a conserved and functionally important tryptophan W427 relative to the binding site of NAD$^+$.

(**B**) Zoom in the cryo-EM structures of hsNADK. Side-chains of hydrophobic residues (F418, L421 from one monomer and F355' and I358' from a second monomer) in contact with the tryptophan W427 are shown in stick, while the remaining of the structure is shown as ribbons.

(**C**) Zoom in the cryo-EM structures of hsNADK. Side-chains of the conserved asparagine N428 (following W427) and those of the interacting residues (T309', T310' and S352' from a second monomer) are shown in stick, while the remaining of the structure is shown as ribbons.

(**D**) Comparison of the C-termini of hsNADK and yeast POS5 (PDB3AFO). The NAD$^+$-bound structure of hsNADK$_{esv}$ and the NAD$^+$-bound form of POS5 are shown in orange and cyan, respectively. The tryptophan W427 and arginine R430 and the equivalent residues in yeast POS5 (F400 and F404) are shown in stick.

(**E**) Zoom in the region of the C-tail of hsNADK, highlighting the positions of the bound NAD$^+$ molecules and conserved functionally important residues (W427, R430) that are visible in the cryoEM structures of hsNADK. The protein is shown as grey ribbons while the NAD$^+$ and the side-chains of W427 and R430 are shown in orange sticks. The electron density from hsNADK$_{esv}$-NAD$^+$ is shown in orange surface.

(**F**) Hybrid model of C-tail of hsNADK. Zoom in the region of C-tail of hsNADK highlights the positions of conserved functionally important residues (W427, R430, Q433, and F436). The C-tail predicted by Alphafold was slightly reoriented to fit into the residual density of hsNADK$_{FL}$-apo. The C-terminal helix and tail are shown in dark-green ribbons, while the hybrid model is in blue ribbons. The extra electron density from hsNADK$_{FL}$-apo is shown in cyan surface. Panels A-F are drawn using PyMOL.

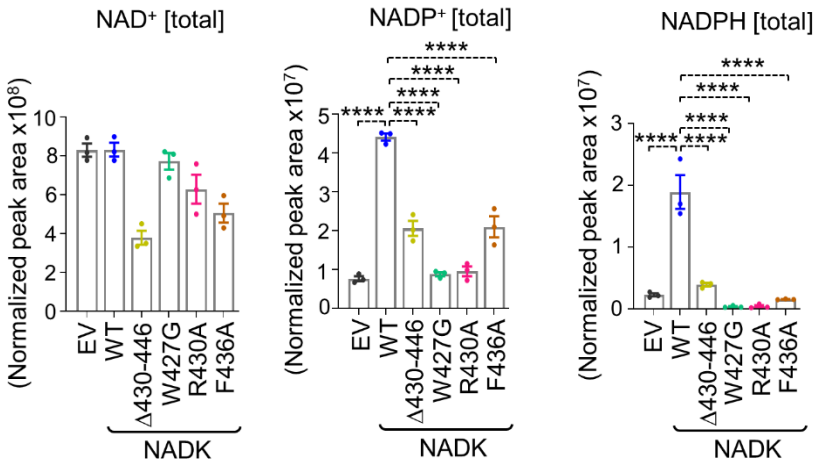

Fig. S8. Effects of the C-terminal NADK mutations on cellular NAD(P)(H) pools.

Normalized peak areas showing total NAD^+, $NADP^+$, and NADPH pools from NADK-deficient HEK-293 cells expressing either empty vector (EV) or the indicated NADK variants (WT, Δ430-446, W427G, R430A, and F436A). All the data are shown as the mean ± S.E.M. of biological triplicates from at least two independent experiments. ****$p < 0.0001$ was calculated with one-way ANOVA and Sidak Post-hoc test.

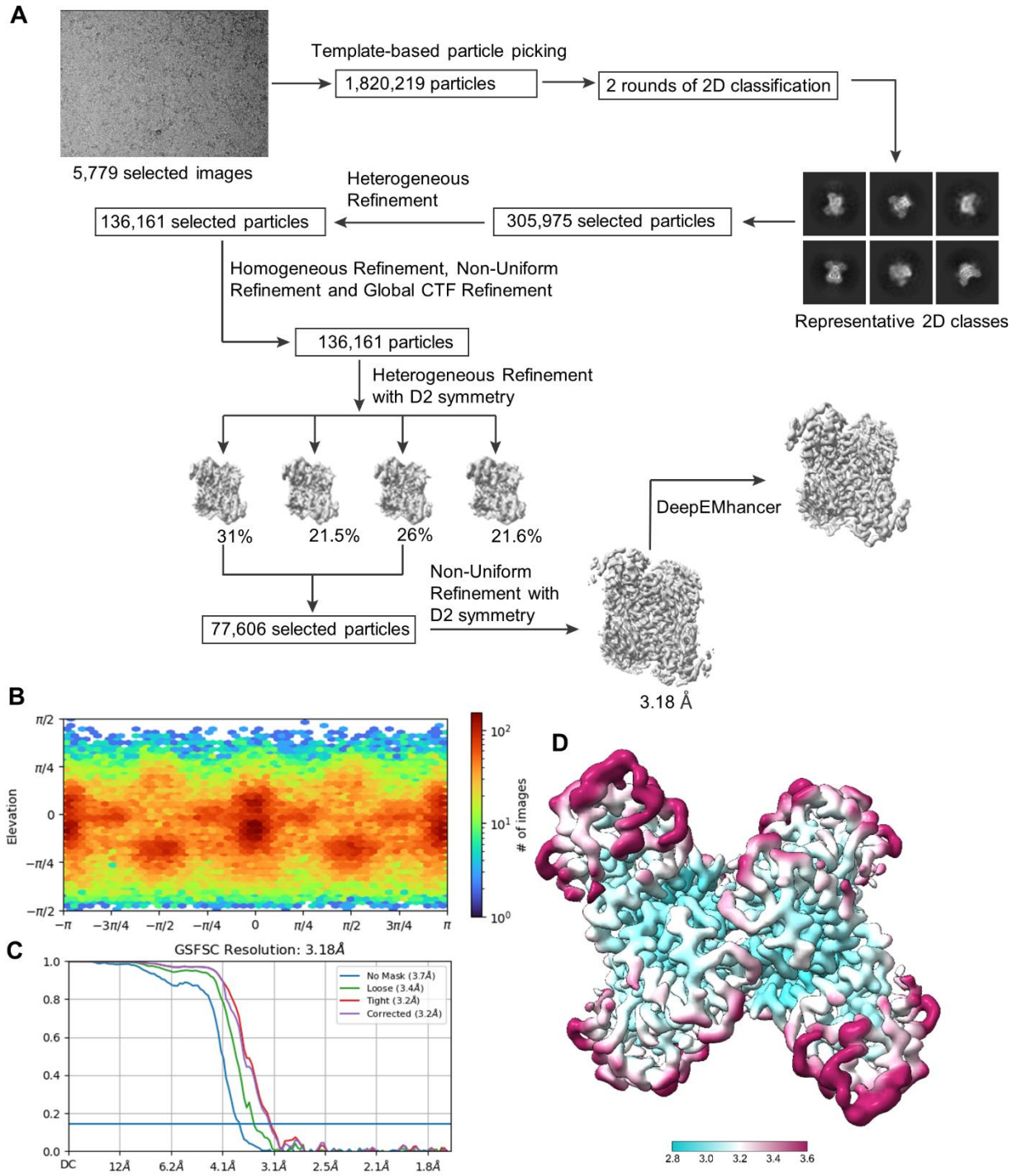
A
5,779 selected images
Template-based particle picking
1,820,219 particles
2 rounds of 2D classification
Representative 2D classes
305,975 selected particles
Heterogeneous Refinement
136,161 selected particles
Homogeneous Refinement, Non-Uniform Refinement and Global CTF Refinement
136,161 particles
Heterogeneous Refinement with D2 symmetry
31%
21.5%
26%
21.6%
77,606 selected particles
Non-Uniform Refinement with D2 symmetry
DeepEMhancer
3.18 Å
B
Elevation
# of images
C
GSFSC Resolution: 3.18Å
No Mask (3.7Å)
Loose (3.4Å)
Tight (3.2Å)
Corrected (3.2Å)
D

Figure S9: Cryo-EM image processing for $NADK_{FL}$.

(**A**) Flowchart of the cryo-EM data processing of $NADK_{FL}$.

(**B**) The Euler angle distribution plot from cryoSPARC.

(**C**) The gold-standard Fourier shell correlation (GS-FSC) curves from cryoSPARC.

(**D**) Local resolution estimation of the cryo-EM map of $NADK_{FL}$.

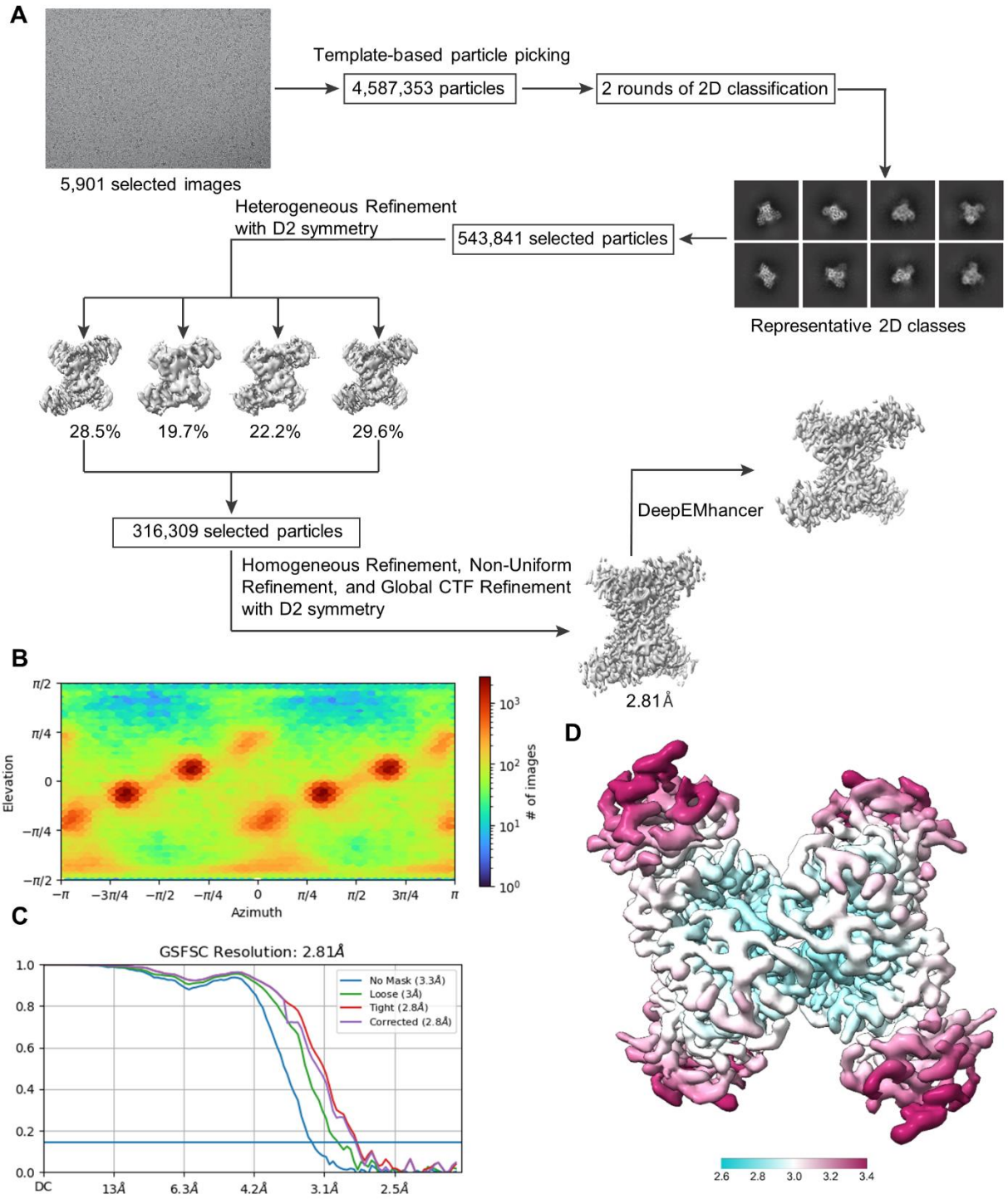
A
Template-based particle picking
4,587,353 particles
2 rounds of 2D classification
5,901 selected images
Representative 2D classes
543,841 selected particles
Heterogeneous Refinement
with D2 symmetry
28.5%
19.7%
22.2%
29.6%
316,309 selected particles
Homogeneous Refinement, Non-Uniform
Refinement, and Global CTF Refinement
with D2 symmetry
DeepEMhancer
2.81Å
B
Elevation
Azimuth
# of images
C
GSFSC Resolution: 2.81Å
No Mask (3.3Å)
Loose (3Å)
Tight (2.8Å)
Corrected (2.8Å)
D

Figure S10: Cryo-EM image processing for $NADK_{esv}$.

(**A**) Flowchart of the cryo-EM data processing of $NADK_{esv}$.

(**B**) The Euler angle distribution plot from cryoSPARC.

(**C**) The gold-standard Fourier shell correlation (GS-FSC) curves from cryoSPARC.

(**D**) Local resolution estimation of the cryo-EM map of $NADK_{esv}$.

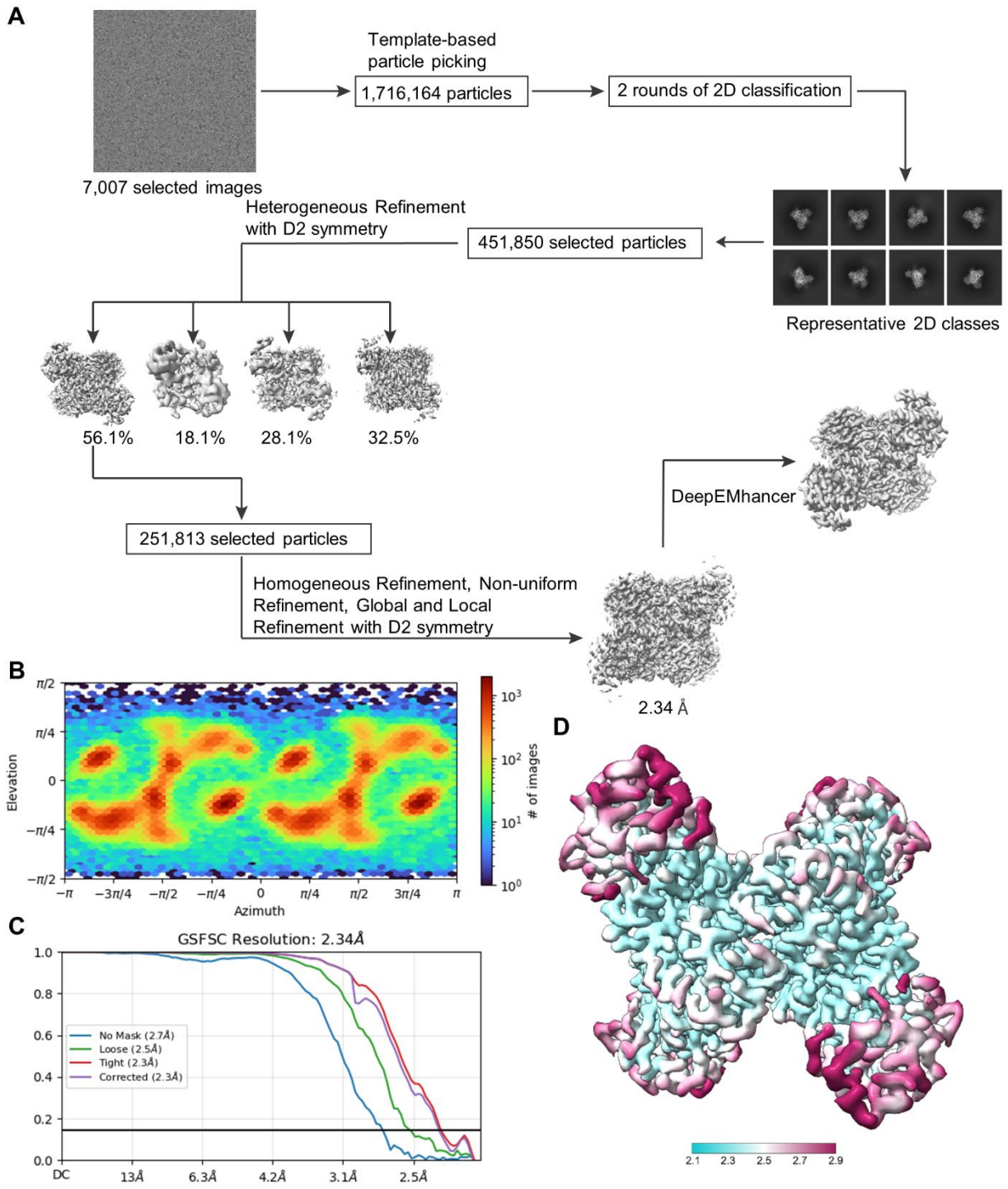
A
Template-based particle picking
1,716,164 particles
2 rounds of 2D classification
7,007 selected images
Representative 2D classes
Heterogeneous Refinement with D2 symmetry
451,850 selected particles
56.1%
18.1%
28.1%
32.5%
DeepEMhancer
251,813 selected particles
Homogeneous Refinement, Non-uniform Refinement, Global and Local Refinement with D2 symmetry
2.34 Å
B
Elevation
Azimuth
# of images
C
GSFSC Resolution: 2.34Å
No Mask (2.7Å)
Loose (2.5Å)
Tight (2.3Å)
Corrected (2.3Å)
D

Figure S11: Cryo-EM image processing for $NADK_{esv}$-NAD^+.

(**A**) Flowchart of the cryo-EM data processing of $NADK_{esv}$ -NAD+.

(**B**) The Euler angle distribution plot from cryoSPARC.

(**C**) The gold-standard Fourier shell correlation (GS-FSC) curves from cryoSPARC.

(**D**) Local resolution estimation of the cryo-EM map of $NADK_{esv}$-NAD^+.